Ocean Engineering 280 (2023) 114579

Contents lists available at ScienceDirect

Ocean Engineering

journal homepage: www.elsevier.com/locate/oceaneng

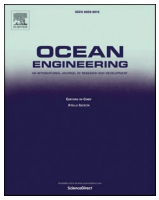

Short-term analysis of extreme wave-induced forces on the connections of a floating breakwater

A.J. Cebada-Relea, M. López *, R. Claus, M. Aenlle

DyMAST Research Group and Department of Construction and Manufacturing Engineering, University of Oviedo, Polytechnic School of Mieres, 33600, Mieres, Asturias, Spain

ARTICLE INFO

Handling Editor: Prof. A.I. Incecik

Keywords:
Floating breakwater
Short-term analysis
Extreme loads
Numerical modelling
Aqwa

ABSTRACT

In the design of floating breakwaters, assessment of the extreme wave-induced loads on the connections, their weakest element, is required to ensure structure survival. This case study provides guidelines for estimating the extreme wave-induced forces on the connections of a floating breakwater. A Boundary Element Method (BEM) solver was applied to obtain the time-domain response of an array of five pontoons anchored to the sea bottom with elastic mooring lines. The hydrodynamic behaviour of the structure was assessed for short-duration sea states with different wave peak periods and oblique wave directions. Two peak selection criteria were applied to obtain force distributions, and several different probability density functions (PDF) were fitted to the resulting data. The extreme wave-induced forces on every connection and sea state were estimated for two different exceedance levels during a typical 3-h sea state. Based on the results, combination of the Peaks Over Threshold (POT) method and generalized Pareto distribution results is proposed for estimating the wave-induced design forces on the connections of floating pontoon breakwaters.

1. Introduction

Floating breakwaters are considered an economical and eco-friendly alternative to their bottom-founded counterparts (Dai et al., 2018). These structures are deployed to provide shelter in low wave energy environments, such as inner harbour basins or recreational marinas (McCartney, 1985). Although floating breakwaters have been designed and constructed in a wide range of configurations and forms, they usually consist of an array of floating modules moored to the seabed by catenary chains or elastic lines (Fig. 1). This study focused on the pontoon subtype, also referred to as double-pontoon, twin-pontoon, or catamaran-type because of the typical shape of its modules.

Floating pontoon breakwater performance has been demonstrated to be satisfactory, however, the connections between the modules, which have a high failure rate (Ferreras et al., 2014), are their "Achille's Heel" (Richey, 1982). The typical connection is composed of wire ropes and rubber fenders, which are intended to withstand tensile and compression forces, respectively (Fig. 2). The failure mechanism is in the wire ropes, which are unable to withstand the wave-induced forces during extreme sea-states. Wave directionality has a noticeable impact on these forces, and critical conditions tend to occur during oblique sea states (Peña et al., 2011; Diamantoulaki and Angelides, 2010). The wave period and the position of the connection in the array also influence the maximum forces on the connections to a great extent (Diamantoulaki and Angelides, 2010; Martinelli et al., 2008). In addition to being critical structural elements, connection stiffness conditions the performance of the whole structure (Martinelli et al., 2008). Therefore, an exhaustive analysis of the wave-induced forces is required for a proper design of floating pontoon breakwaters.

The wave-induced forces on the connections can be found by numerical modelling. Several 2-D frequency-domain linear models have been applied to study the interaction of floating breakwaters and waves, mainly by finite elements (Elchahal et al., 2009), the element-free Galerkin method (Lee and Cho, 2003), and the boundary element method (BEM) (Williams et al., 2000). Nonetheless, since wave obliquity is directly related to the forces on the connectors, 3-D models are required to account for it, and have been widely applied to simulate floating breakwaters with layouts of differing complexity. Some examples include a standalone moored pontoon (Loukogeorgaki and Angelides, 2005), a free-floating breakwater consisting of hinged modules (Diamantoulaki and Angelides, 2010), and the more realistic case of a hinged cable-moored floating breakwater (Diamantoulaki and

* Corresponding author.
E-mail address: mario.lopez@uniovi.es (M. López).

https://doi.org/10.1016/j.oceaneng.2023.114579
Received 21 February 2023; Received in revised form 29 March 2023; Accepted 12 April 2023
Available online 3 May 2023

Fig. 1. Pontoon-type floating breakwater in the Port of Figueras (Asturias, Spain).

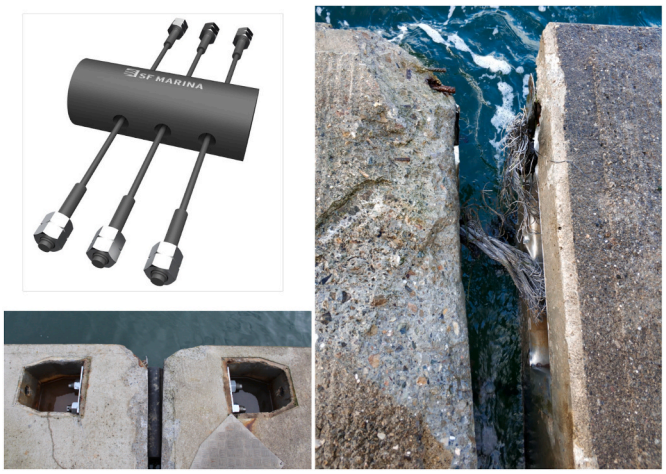

Fig. 2. Semi-rigid floating breakwater connector type (Marina) (upper left), connection installed and working properly (lower left) and broken connection after sea storms (right).

Angelides, 2011). Frequency-domain analysis relies on linearization of the hydrodynamic loads and the system response, and therefore, time-domain simulations are preferred, their higher computational cost notwithstanding (Stanisic et al., 2017). Chen et al. (2017) analysed the response of a moored floating pontoon under regular waves with a 3D model and found good agreement with experimental tests in a wave tank. Regular sea state simulation requires less computational effort than irregular sea states. However, this approach should be applied with caution, as the wave-induced forces on the connections tend to be underestimated (Cebada-Relea et al., 2022a). On this basis, 3D time-domain simulations of irregular sea states are the most appropriate approach for solving the hydrodynamics of floating pontoon breakwaters and finding the wave-induced forces on their connections.

Once the time series of wave-induced forces are found for a given sea state by numerical modelling, their statistical analysis commonly follows. Although the literature in this regard for floating breakwater connections is scarce, there are abundant examples related to the mooring lines of floating structures. For example, Dunja et al. (Stanisic et al., 2018) analysed the peak events on the mooring system of a vessel model subjected to a tropical cyclone environment. The short-term extreme response of a semi-submersible design was also analysed by Sheng et al. (Xu and yanGuedes Soares, 2019). In this study, a hybrid mooring configuration was found using the average conditional exceedance rate method, the global maxima method and the Peaks Over Threshold (POT) method to assess the extreme forces on these elements. Furthermore, previous studies on a scaled point absorber wave energy converter with hybrid mooring have found that generalized Pareto and gamma distributions are suitable for fitting a mooring system peak (Xu et al., 2020; Xu and Guedes Soares, 2021). Other recent studies have also included estimation of the extreme response in complex environments, including station-keeping trials in ice (e.g. (Zhao et al., 2021; Sinsabvarodom et al., 2021)).

Extreme value analysis of a given sea state usually requires a long enough time series and an adequate sampling rate, and especially, multiple simulations or repetitions (Agarwal et al., 2015). The simplest approach is to find the maximum value for each time-domain simulation and select the design load from such statistical quantities as the mean, the most probable maximum (MPM) or a given percentile. However, this approach may be unfeasible for the design of floating pontoon breakwaters, which require time-consuming 3D simulations in the time domain of irregular sea states, for two major reasons. First, sea state duration must be 20 min to 6 h to ensure process stationarity, although a 3-h duration is typically assumed for standardized design procedures (DNV GL, 2017). If only a single peak from each repetition were considered, too many repetitions would be required to obtain accurate statistics (Stanisic et al., 2017, 2018; Zhao et al., 2021). Second, repetition of 3-h simulations requires execution times that are too long. Therefore, some alternative approaches have been proposed for analysing marine structures other than floating breakwaters. For example, Agarwal et al. (2015) used more than one peak per repetition to fit the values to a probability distribution and estimate extreme events. Stanisic et al. (2018) applied the opposite method and estimated the design loads of vessel mooring lines from a single long time simulation.

This study proposed and applied a complete methodology for estimating short-term design forces on the connections of floating pontoon breakwaters from short simulations. The time series of wave-induced forces on the connections of a floating breakwater in this case study were found with a 3D BEM numerical model. A total of nine irregular sea states with different wave peak periods and wave heading angles were analysed. Two peak selection criteria were applied, and different probability density functions were used to fit each dataset. Then, the wave-induced forces for different exceedance probabilities in a typical 3-h sea state were found with the two fits. Some guidelines based on analysis and discussion of the results are provided for the design of floating breakwaters.

The remainder of the paper is structured as follows. Section 2 describes the pontoon array and its main properties, the numerical model scheme, and the short-term statistics applied to fit the results from the simulations and estimate the 3-h extreme forces on the connections. The results are presented and discussed in Section 3, and conclusions are drawn in Section 4.

2. Material and methods

2.1. Case-study breakwater

The breakwater studied consisted of an array of five floating pontoons interconnected with hinged joints and anchored to the seabed with elastic mooring lines at a depth of $d = 6.75$ m. The geometry of the pontoon, its mooring arrangement and its mechanical properties were based on the experimental work of Peña et al. (2011) (Fig. 3).

2.2. Numerical model

The ANSYS Aqwa code was used to simulate the hydrodynamic behaviour of the breakwater. This tool has previously been applied to design a wide variety of marine structures, including: vessels (Rajesh Reguram et al., 2016), wave energy converters (Ramos et al., 2018) and offshore fish cages (Chu et al., 2022). Moreover, Aqwa has already been applied successfully to floating pontoon arrays in regular waves (Chen et al., 2017; Samaei et al., 2016), and more recently, in irregular waves (Cebada Relea et al., 2022; Cebada-Relea et al., 2022b). The numerical modelling scheme and the simulated sea states are described below.

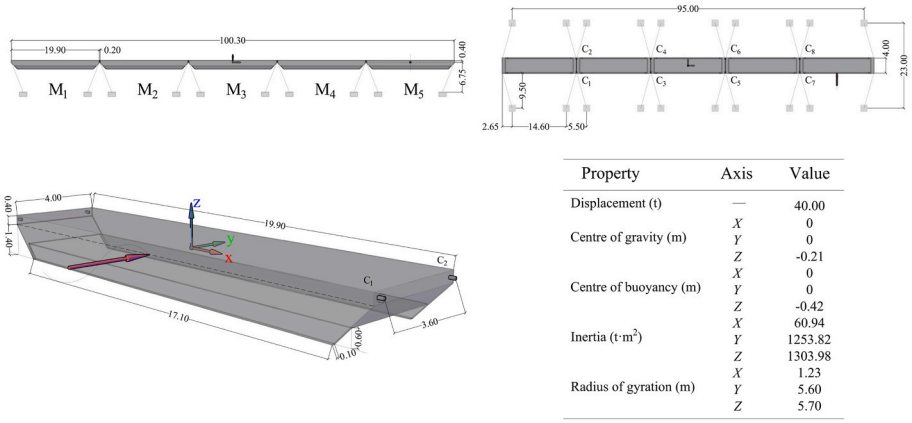

Property	Axis	Value
Displacement (t)	—	40.00
Centre of gravity (m)	X	0
	Y	0
	Z	-0.21
Centre of buoyancy (m)	X	0
	Y	0
	Z	-0.42
Inertia (t·m^2)	X	60.94
	Y	1253.82
	Z	1303.98
Radius of gyration (m)	X	1.23
	Y	5.60
	Z	5.70

Fig. 3. Main floating breakwater elements and dimensions [m]. M_m (with m = 1,2, …,5) is the module reference, and C_n (with n = 1,2, …,8) is the connection reference. Based on (Peña et al., 2011).

2.2.1. Numerical modelling scheme

Time-domain simulations in both regular and irregular waves were performed with Aqwa Naut (ANSYS, 2016). The forces on the array were recomputed using a two-stage predictor-corrector algorithm to estimate the positions, velocities, and accelerations of the modules at each time step. The variation in the instantaneous wetted surface of the modules was also included to account for nonlinear hydrodynamic effects. Fig. 4 shows the meshed geometry of a module, featuring the panels above and below the mean water level. A total of 16,000 (0.30 ± 0.1-m) quadrilateral panels were used to mesh the complete array geometry. The results of the mesh convergence analysis are presented under Results.

The motion equation in the time domain is:

$$\mathbf{M}\cdot\ddot{\mathbf{x}}(t) = \mathbf{f}_h(t) + \mathbf{f}_I(t) + \mathbf{f}_d(t) + \mathbf{f}_r(t) + \mathbf{f}_c(t) + \mathbf{f}_m(t) \tag{1}$$

where $\mathbf{x}(t)$ is the displacement from the hydrostatic equilibrium position and $\mathbf{M}$ is the mass matrix of a floating pontoon. This accounts for the hydrostatic $\mathbf{f}_h(t)$, incident wave or Froude-Krylov $\mathbf{f}_I(t)$, diffraction $\mathbf{f}_d(t)$, radiation $\mathbf{f}_r(t)$, connection $\mathbf{f}_c(t)$ and mooring $\mathbf{f}_m(t)$ forces.

The nonlinear hydrostatic force $\mathbf{f}_h(t)$ is calculated as the balance between gravitational forces $\mathbf{f}_g(t)$ and the upward buoyant force. The hydrostatic force, considering the pontoon's instantaneous wetted surface $S(t)$, is given by the following equation:

$$\mathbf{f}_h(t) = \mathbf{f}_g(t) + \rho g \int_{S(t)} p_{st}(t)\mathbf{n}dS \tag{2}$$

where $p_{st}(t)$ is the instantaneous static pressure, ρ is the sea water density, g is the gravity acceleration and $\mathbf{n}$ is the unitary normal vector.

Incident wave forces $\mathbf{f}_I(t)$ are also dependant on the instantaneous wetted surface and are estimated for each time step as

$$\mathbf{f}_I(t) = \int_{S_i} p_{dyn}(t)\ \mathbf{n}dS, \tag{3}$$

where the Wheeler stretching method (Elchahal et al., 2009) is applied to determine the dynamic body pressure $p_{dyn}(t)$.

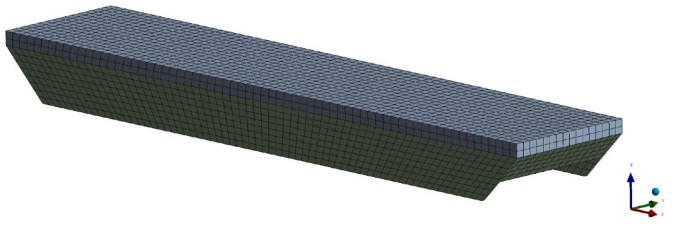

Fig. 4. Meshed geometry of a floating pontoon unit. Green panels are below the mean wetted surface and and grey above.

Diffraction forces, including contributions from all the diffracting panels (those contained in the mean wetted surface, S_0) are computed as:

$$\mathbf{f}_d(t) = -\int_{S_0} p_d(t)\ \mathbf{n}dS \tag{4}$$

where p_d is the diffraction pressure, which is dependent on angular frequency (ω) and can be defined as follows:

$$p_d(t) = i\omega\rho\varphi_d e^{-i\omega t}. \tag{5}$$

The "memory effect" is captured by the radiation force term $\mathbf{f}_r(t)$ (Cummins, 1962):

$$\mathbf{f}_r(t) = -\mathbf{A}_\infty\ddot{\mathbf{x}}(t) - \int_0^t \mathbf{H}(t-\tau)\cdot\ddot{\mathbf{x}}(\tau)d\tau, \tag{6}$$

where $\mathbf{A}_\infty$ is the added mass for an infinite frequency, and $\mathbf{H}$ is the impulse-response function:

$$\mathbf{H}(t) = \frac{2}{\pi}\int_0^\infty \mathbf{B}(\omega)\frac{sin(\omega t)}{\omega}d\omega = \frac{2}{\pi}\int_0^\infty [\mathbf{A}(\omega) - \mathbf{A}_\infty]cos(\omega t)\ d\omega \tag{7}$$

$\mathbf{A}$ is the added mass, and $\mathbf{B}$ is the potential damping. These hydrodynamic coefficients were adopted from a previous frequency domain analysis based on potential flow theory (Cebada-Relea et al., 2022a).

$\mathbf{f}_m(t)$ accounts for the forces on the mooring lines (linear-elastic cables):

$$\mathbf{f}_m(t) = \begin{cases} 0 & \text{if } L(t) \le L_0 \\ K_m(L(t) - L_0) & \text{if } L(t) > L_0 \end{cases}, \tag{8}$$

where $L(t)$ is the instantaneous cable length, L_0 is the starting cable length, and K_m = 30 kN/m is the mooring line stiffness assuming 30% line pretension (Peña et al., 2011).

$\mathbf{f}_c(t)$ accounts for the forces in connection elements C_n (Fig. 3). The longitudinal component is hereinafter referred to as T. At both ends of each connection, there is a hinged joint that transfers forces and restores moments between modules:

$$\mathbf{M} = -\begin{bmatrix} K_{rx} & 0 & 0 \\ 0 & K_{ry} & 0 \\ 0 & 0 & K_{rz} \end{bmatrix}[0, \mathbf{G}^\mathbf{T}]\left[\mathbf{U_p} - \mathbf{U_c}\right], \tag{9}$$

where K_{rx}, K_{ry} and K_{rz} are the rotational stiffness around the principal axes, $\mathbf{G}^\mathbf{T}$, is the unitary change-of-basis matrix from the local joint axes to the main axes, and $\mathbf{U_p}$ and $\mathbf{U_c}$ are the translation and rotation matrices of the pontoon and connectors, respectively. Note that because of the geometrical arrangement (two connections between each pair of modules), the relative translations are restrained and only relative rotation around the Y axis is possible. Joint stiffness, K_{ry}, and the viscous

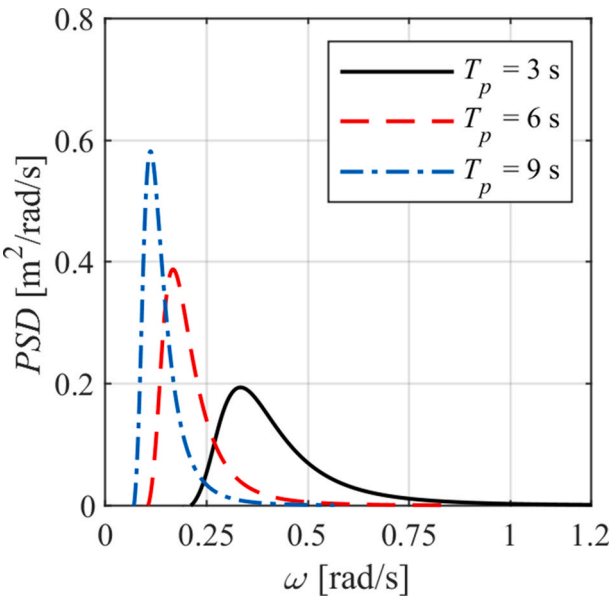

Fig. 5. Pierson-Moskowitz PSD used for the irregular sea state simulations.

damping of the pontoon fins were calibrated by Cebada et al. (Cebada-Relea et al., 2022a) based on experimental results found by Peña et al. (2011).

2.2.2. Irregular sea states and repetitions

A total of nine long-crested irregular sea states, corresponding to a combination of three wave headings of $\theta = 22.5$, 45.0 and 67.5°, where $\theta = 90.0°$ is a wave perpendicular to the breakwater alignment, and three wave spectral peak periods of $T_p = 3$, 6 and 9 s were included. All sea states had the same significant wave height of $H_s = 0.85$ m. In a compromise between accuracy and computation time, the duration of the simulations was set to 2000 s and the time step to 0.01 s.

The Pierson-Moskowitz power spectral density (PSD) (Fig. 5) was used for modelling irregular waves,

$$PSD(\omega) = \frac{4\pi^3}{\omega^5}\frac{H_s^2}{\left(1.408\cdot T_p\right)^4} e^{\left(\frac{16\pi^3}{\omega\left(1.408\cdot T_p\right)^4}\right)}. \tag{10}$$

The wave amplitude of each harmonic constituent was found from the PSD for each sea-state, and the wave phases were pseudo-randomly assigned by means of predefined seeds. To capture inherent wave randomness, 20 repetitions of each sea-state were performed with different seeds (DNV GL, 2018) (Fig. 6).

2.3. Short-term extreme value analysis

Twenty repetitions were performed with different random seeds (as described in Section 2.2.2 above). The wave-induced force distributions found from the short-duration time series were then used to develop 3-h force distributions, and finally, to estimate the corresponding design value.

2.3.1. Force peak selection

One of the major issues in exploration of a short-term extreme distribution is the definition and selection of peaks, which are assumed to be random and statistically independent of each other. The zero-up crossing and the Peaks Over Threshold (POT) methods were used for peak selection (Fig. 7). The former defines a peak as the maximum load between two successive zero-up crossings in the time series. The POT method defines a peak as the maximum load within a time window (to ensure independence of the peaks) that is above a given threshold. Although there are no well-established rules for the selection of this threshold, it is usually within the 50th to 95th percentiles of all peak values (Zhao et al., 2021).

2.3.2. Probability distribution models

Since no studies on short-term distribution of the forces on the connections of floating breakwaters are available, the data retrieved form the simulations were fitted using different probability density functions (PDFs). The maximum likelihood method was used to adjust the parameters of each function. Goodness of fit was achieved by means of the normalized root mean square error (NRMSE). The PDFs considered are presented below.

- Weibull PDF,

$$f(x|a_{WB}, b_{WB}) = \frac{b_{WB}}{a_{WB}}\left(\frac{x}{a_{WB}}\right)^{b-1} e^{-\left(\frac{x}{a_{WB}}\right)^{b_{WB}}} \tag{11}$$

where a_{WB} is the scale parameter and b_{WB} the shape parameter.

- Rayleigh PDF,

$$f\left(x\middle|b_{Ray}\right) = \frac{x}{{b_{Ray}}^2} e^{\left(\frac{-x^2}{2{b_{Ray}}^2}\right)} \tag{12}$$

where b_{Ray} is the shape parameter.

- Gamma PDF,

$$f(x|a_{GM}, b_{GM}) = \frac{1}{{b_{GM}}^{a_{GM}}\Gamma(a_{GM})} x^{a_{GM}-1} e^{\frac{-x}{b_{GM}}} \tag{13}$$

where a_{GM} is the shape parameter, b_{GM}, the scale parameter, and Γ the gamma function.

- Generalized Pareto PDF,

$$f(x|k_{GP}, \sigma_{GP}, u_{GP}) = \left(\frac{1}{\sigma_{GP}}\right)\left(1 + k_{GP}\frac{(x-u_{GP})}{\sigma_{GP}}\right)^{-1-\frac{1}{k_{GP}}} \tag{14}$$

where k_{GP} is the shape parameter, σ_{GP}, the scale parameter, and μ_{GP}, the threshold.

- Generalized Extreme Value PDF,

$$f(x|k_{GEV}, \sigma_{GEV}, \mu_{GEV}) = \left(\frac{1}{\sigma_{GEV}}\right) e^{\left(-\left(1+k_{GEV}\frac{(x-\mu_{GEV})}{\sigma_{GEV}}\right)^{-\frac{1}{k_{GEV}}}\right)} \ldots\ldots \left(1 + k_{GEV}\frac{(x-\mu_{GEV})}{\sigma_{GEV}}\right)^{-1-\frac{1}{k_{GEV}}} \tag{15}$$

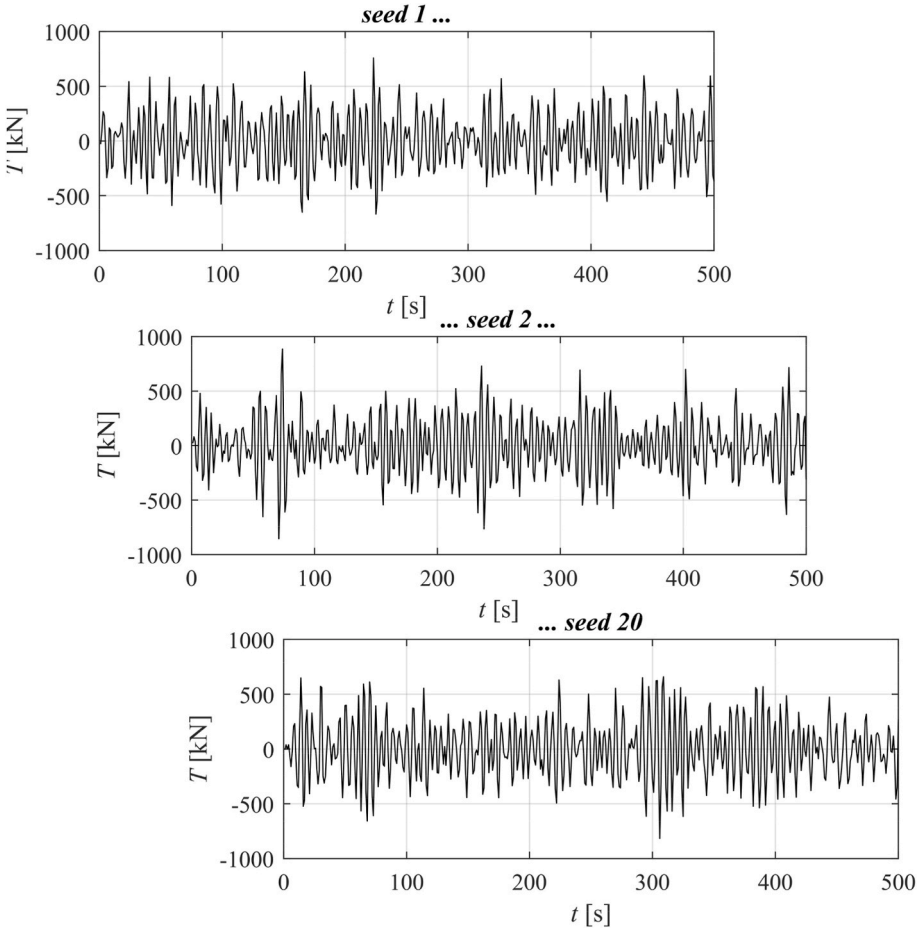

Fig. 6. Time series of wave-induced forces for sea-state 6 found with different seeds.

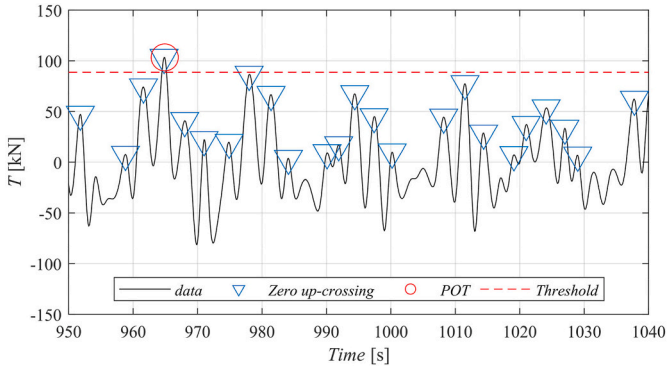

Fig. 7. Example of peak selection with the zero-up crossing and Peakd Over Threshold (POT) methods. The time series is for sea-state 5 ($H_s = 0.85$ m, $T_p =$ 6s and $\theta = 45°$) and Connection C_3.

where k_{GEV} is the shape parameter, σ_{GEV} the scale parameter and μ_{GEV} is the location parameter.

- Half-Normal PDF,

$$f(x|\sigma_{HN},\mu_{HN}) = \sqrt{\frac{2}{\pi}}\frac{1}{\sigma_{HN}}e^{-\frac{1}{2}\left(\frac{x-\mu_{HN}}{\sigma_{HN}}\right)^2} \tag{16}$$

where σ_{HN} is the shape parameter and μ_{HN} is the location parameter.

- Loglogistic PDF,

$$f(x|\sigma_{LG},\mu_{LG}) = \frac{1}{\sigma_{LG}}\frac{1}{x}\frac{e^z}{(1+e^z)^2}, \tag{17}$$

for

$$z = \frac{\log(x)-\mu_{LG}}{\sigma_{LG}}, \tag{18}$$

where σ_{LG} is the scale parameter and μ_{HN} is the location parameter.

2.3.3. 3-H extreme value analysis

The exceedance probability of a given wave-induced force in a 3-h sea-state was found as one minus the cumulative density function (CDF):

$$F_{3h}(x) = 1 - \int_0^{\infty} f(x)^{n_{3h}}dx, \tag{19}$$

where $f(x)$ is the PDF fitted to the peak data found from the short-duration time series, and n_{3h} is the expected number of peaks in a 3-h sea state. The latter parameter was simply obtained as

$$n_{3h} = 5.4n, \tag{20}$$

where n is the average number of peaks in a short-duration time series, which depends on the peak selection criterion and the ratio of 3-h to the duration of the simulations analysed.

In the Most Probable Maximum approach (MPM), the modal value (or mode) of the datasets, which has a 63% probability of exceedance, is usually considered the design value (Stanisic et al., 2017; Xu and yan-Guedes Soares, 2019; Cheng and Kuang, 2016). Other approaches

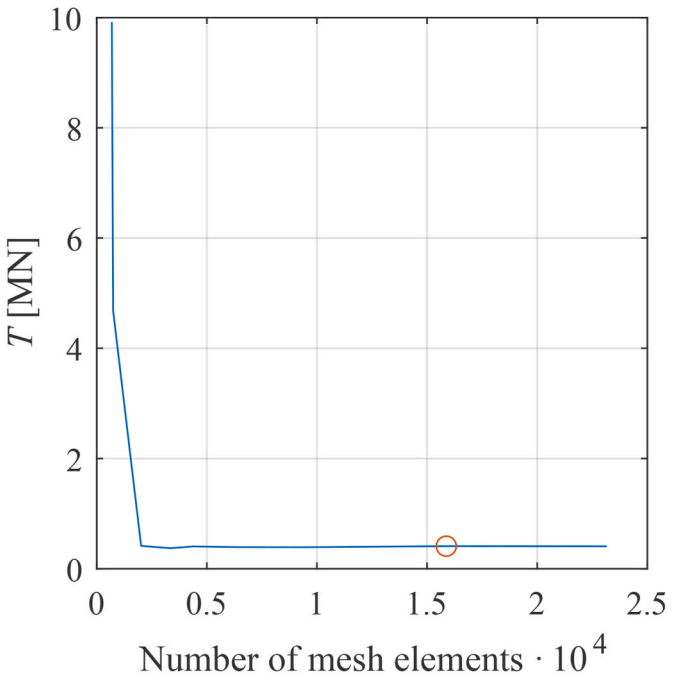

Fig. 8. Results of mesh convergence analysis. The red circle marks the number of elements selected.

consider the 90th percentile of upper values, i.e. 10% probability of exceedance (Stanisic et al., 2017). Accordingly, two of the design force values in each 3-h sea state were found by solving Eq. (19) for $F_{3h} = 0.63$ and 0.10, $T_{0.63}$ and $T_{0.10}$, respectively.

3. Results and discussion

This section explores the wave-induced forces in the floating pontoon breakwater. The simulation results for irregular oblique sea states are presented in terms of the peak wave-induced forces on the connections between modules, which were fitted to well-established probability models. Two different peak selection approaches were applied and compared: zero-up crossing and Peaks Over Threshold (POT). Finally, the design forces for the 3-h sea states are estimated and discussed.

3.1. Mesh convergence analysis

Prior to any analysis, a mesh sensibility analysis was carried out to ensure the independence of the results of the mesh. As an example, Fig. 8 plots the values of the maximum wave-induced force (T) on Connection C_3, found after simulating Sea State 3 ($T_p = 3$ s, $H_s = 0.85$ m, and $\theta = 67.5°$) with different numbers of mesh elements. As shown, mesh independence is ensured for the element size and number of elements (0.30 ± 0.1 m and 16,000, respectively, as in Section 2.2.1) considered.

3.2. Wave-induced force peaks

The behaviour of the floating breakwater in irregular oblique waves was simulated with the numerical modelling approach described in Section 2.2.1. The sea states were defined after combining $T_p = 3$, 6 and 9 s and $\theta = 22.5$, 45.0 and 67.5° in a common significant wave height of $H_s = 0.85$ m, and modelled with the Pierson-Moskowitz spectrum according to Eq. (10) (Fig. 5). Each sea state was simulated 20 times with different spectral wave phases (seeds) to capture wave randomness. The time series of wave-induced forces were retrieved for each simulation and for each connection in the array. To guarantee statistical independence, only force peaks in the time series were considered in the following probability analysis. The zero-up crossing and POT methods were used for peak selection. The results of these two methods are presented and discussed below.

3.2.1. Peaks selected with the zero-up crossing method

First, the wave-induced force peaks were selected with the zero-up crossing method. From 4,000 to 12,000 peaks were identified for each sea state in all 20 repetitions (Table 1). Wave conditions, and in particular, the peak period (T_p) and the wave heading angle (θ), significantly influenced the forces on the connection. For example, the mean force on connection C_3 varied from $\overline{T} = 79.7$ (Sea State 1, $T_p = 3$ s and $\theta = 22.5°$) to $\overline{T} = 1260.5$ kN (Sea State 9, $T_p = 9$ s and $\theta = 67.5°$). It is apparent that the forces on the connections increase both with increasing T_p and θ in the range of sea states included in this study.

All the sea states showed a clear unimodal right-skewed distribution of wave-induced forces (Fig. 9). The relative standard deviation from the mean (RSD) is very similar for all the sea states (Table 1), revealing a common pattern, as the distribution spread is independent of wave conditions. Similar results were found for all the breakwater connections.

As expected, the range of force peaks varied depending on the position of the connection in the array. An example of force distributions on connections C_1 (between the two first pontoons) and C_3 (between two intermediate pontoons) is shown in Fig. 10. The force peak distribution is narrower for C_1 than for C_3, where force values are higher than for the other. This result reveals that the intermediate connections (C_3, C_4, C_5 and C_6 in Fig. 3) can withstand higher wave-induced forces than the terminal connections (C_1, C_2, C_7 and C_8 in Fig. 3).

3.2.2. Peaks selected using the Peaks Over Threshold (POT) method

The wave-induced force peaks were selected with the Peaks Over Threshold (POT) method considering the 75th percentile of the force peaks found with the zero-up crossing method in the section above as the threshold. This threshold minimizes the Normalized Root Mean Square Error (NRMSE) of fit to the force distributions, as shown in Fig. 11. The peak period of the corresponding sea state was used as the time window

Table 1
Statistiscs of force peaks on connection C_3 found with the zero-up crossing method and Peaks Over Threshold (POT) method. Average force ($\overline{T}$) ± standard deviation, relative standard deviation (RSD) and total number of peaks are included for each sea state.

Sea state			Zero-up crossing			Peaks Over Threshold (POT)		
No.	T_p [s]	θ [°]	$\overline{T}$ [kN]	RSD [%]	No. peaks	$\overline{T}$ [kN]	RSD [%]	No. peaks
1	3	22.5	79.7 ± 47.1	59	10768	106.9 ± 31.0	29	2692
2	3	45.0	117.2 ± 69.3	59	11009	158.2 ± 45.1	29	2752
3	3	67.5	246.0 ± 145.5	59	11503	323.9 ± 99.4	31	2876
4	6	22.5	99.6 ± 58.9	59	7790	143.2 ± 33.1	23	1729
5	6	45.0	233.6 ± 138.2	59	7580	318.5 ± 88.0	28	1760
6	6	67.5	525.5 ± 310.8	59	8205	727.0 ± 191.4	26	1966
7	9	22.5	105.7 ± 62.4	59	6627	150.6 ± 35.8	24	1229
8	9	45.0	273.3 ± 161.4	59	5952	379.4 ± 98.3	25	1296
9	9	67.5	1260.5 ± 739.4	59	9748	1619.4 ± 520.8	32	1481

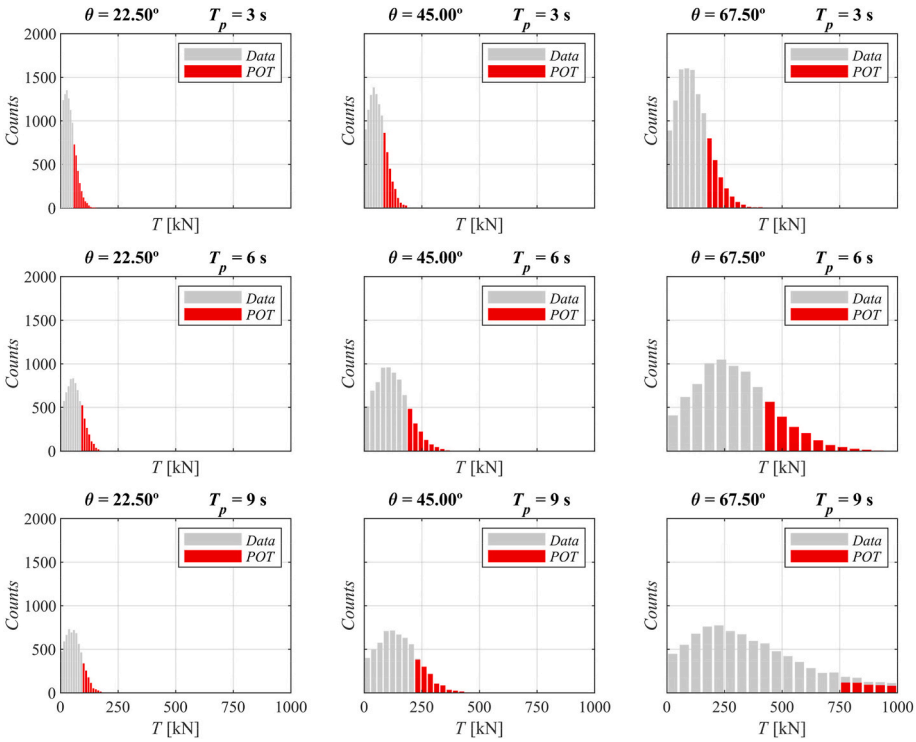

Fig. 9. Histograms of force peaks (T) on Connection C_3 found with the zero-up crossing (grey) and Peaks Over Threshold (POT) (red) methods for each sea state.

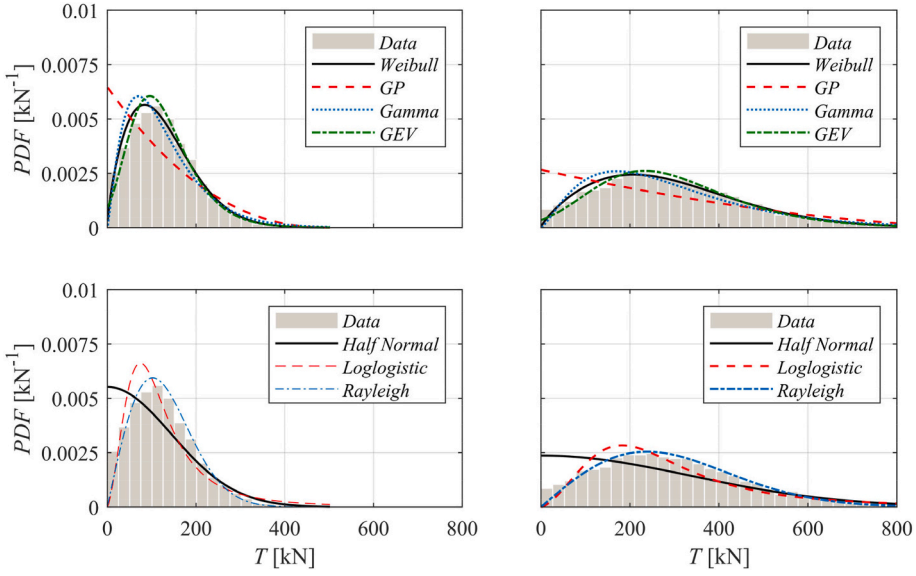

Fig. 10. Histograms of force peaks selected with the zero-up crossing method and fit to probability density functions (PDFs) for Connections C_1 (left) and C_3 (right) at Sea State 6 ($T_p = 6.0$ s and $\theta = 67.5°$).

to ensure that consecutive peak values were independent of each other.

Depending on the sea state, the number of peaks selected with the POT method varied from 1,000 to 3,000, corresponding to an average of 50–150 peaks per simulation (Table 1). Although, as expected, the size of the dataset was significantly smaller than with the zero-up crossing method, it was still large enough for statistical analysis and data fit (Fig. 11).

The POT analysis showed the values of the wave-induced forces (Table 1), confirming the influence of wave conditions and the position of the connection in the array. As expected for an extreme value distribution, the shape of the histograms had a single tail (Fig. 9). Regarding the spread, the POT method results had a lower standard deviation than those found with the zero-up crossing method. Nonetheless, there were wide differences depending on the sea state. For example, distributions corresponding to connection C_3 ranged from RSD = 23% (Sea State 4, $T_p = 6$ s and $\theta = 22.5°$) to 32% (Sea State 9, $T_p = 9$ s and $\theta = 67.5°$) with the POT method, while RSD is nearly constant at around 59% with the zero-up crossing method.

3.3. Peak data fit to PDF

The peak force datasets found with the zero-up crossing method and

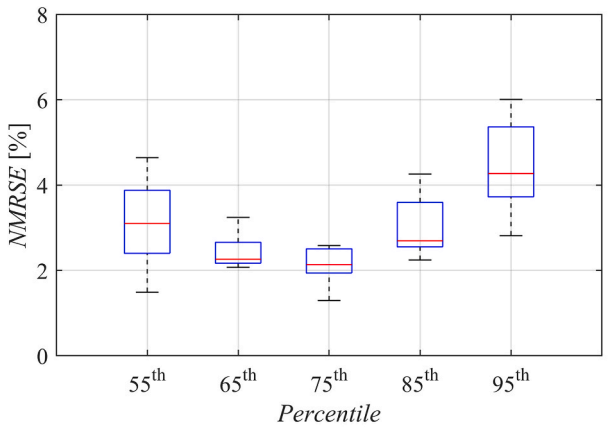

Fig. 11. Normalized Mean Square Error (NRMSE) after fitting the force peaks selected with the POT method to a Pareto PDF as a function of the threshold (expressed as the percentile of force peaks found with the zero-up crossing method). The results are for Sea State 3.

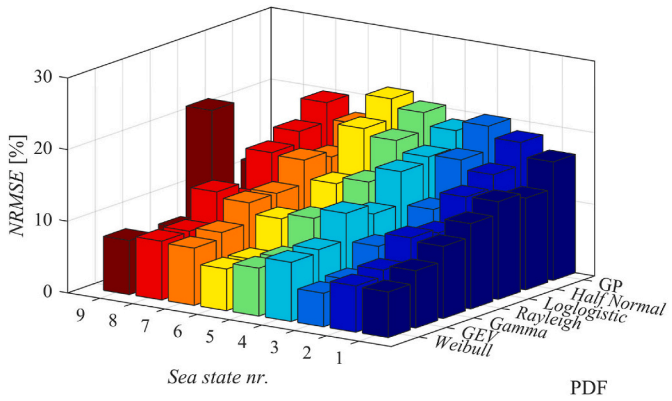

Fig. 12. Average NMRSE between the force peak data obtained with the zero-up crossing method and PDF models at the sea states considered.

the Peaks Over Threshold (POT) method were fitted to the probability density functions (PDFs) defined in Eq. (11) to Eq. (17). The goodness of fit of each PDF to each dataset is presented and discussed below.

3.3.1. Fit of peaks selected with the zero-up crossing method

Fig. 10 shows an example of fit to the force distributions found with different PDFs. Apparently, the Weibull, Rayleigh, gamma and generalized extreme value functions are all suitable for fitting the data with the zero-up crossing method, while the half-normal, loglogistic and generalized Pareto functions are not.

The goodness of fit of each PDF is shown in terms of the NRMSE in Fig. 12. The best fit was usually found with the Weibull distribution with an average NRMSE of about 5%. This PDF fits all the sea states except Sea State 9 the best. The Gamma and Generalized Extreme Value PDFs also had a low NRMSE. The average NRMSE increased to above 15% for the half-normal and the generalized Pareto functions, proving them unsuitable for this fit. Based on this analysis, the Weibull model was selected to fit the force peak data selected with the zero-up crossing method.

Table 2 shows the average parameters of the Weibull distribution (Eq. (11)) for the terminal and intermediate connections. The scale parameter (a_{Wb}) increases with the angle of incidence and the peak period. In addition, its value is higher for intermediate connections, which agrees with the higher wave-induced forces that these connections are subjected to. The average shape parameter (b_{Wb}) varies from 1.1 to 1.8, regardless of the position of the connection or the sea state considered, in accordance with the common pattern previously detected in the distributions.

Table 2
Weibull distribution parameters (average ± standard deviation) found for terminal (C_1, C_2, C_7 and C_8) and intermediate (C_3, C_4, C_5 and C_6) connections.

Sea state			Terminal		Intermediate	
No.	T_p [s]	θ [°]	$\bar{a}_{Wb}$	$\bar{b}_{Wb}$	$\bar{a}_{Wb}$	$\bar{b}_{Wb}$
1	3	22.5	26.11 ± 4.9	1.6 ± 0.1	45.1 ± 2.3	1.5 ± 0.1
2	3	45.0	46.85 ± 5.3	1.7 ± 0.1	68.4 ± 3.2	1.6 ± 0.1
3	3	67.5	96.82 ± 7.2	1.8 ± 0.1	133.3 ± 7.8	1.7 ± 0.1
4	6	22.5	42.52 ± 4.6	1.7 ± 0.1	66.6 ± 2.7	1.6 ± 0.1
5	6	45.0	82.22 ± 5.8	1.8 ± 0.1	135.9 ± 2.4	1.7 ± 0.1
6	6	67.5	143.53 ± 3.8	1.8 ± 0.1	332.5 ± 2.7	1.8 ± 0.1
7	9	22.5	36.64 ± 4.8	1.6 ± 0.1	69.1 ± 3.2	1.6 ± 0.1
8	9	45.0	77.43 ± 4.4	1.7 ± 0.1	161.9 ± 3.8	1.6 ± 0.1
9	9	67.5	289.77 ± 8.9	1.1 ± 0.1	538.5 ± 5.2	1.2 ± 0.1

3.3.2. Fit of peaks selected with the Peaks Over Threshold (POT) method

The fittings of the force distributions found with the POT for a terminal connection (C_1) and an intermediate connection (C_3) are presented in Fig. 13. The goodness of fit of the PDFs is compared in terms of the NRMSE in Fig. 14. In this case the best fit was found with the Generalized Pareto distribution, with an NRMSE of 2–3% for most of the sea-states and connections. The half normal and generalized extreme value distributions also provided a fair fit, while the Weibull, loglogistic, Rayleigh, and Gamma functions are clearly unsuitable for fitting the extreme force peak distribution found using the POT method. As the Generalized Pareto distribution performed better than any other function considered at all sea-states and for all the connections, it was selected for the subsequent extreme value analysis of the wave-induced forces on the connections.

The statistics of the Generalized Pareto function parameters (Eq. (14)) for the terminal (C_1, C_2, C_7, C_8) and intermediate connections (C_3, C_4, C_5 and C_6) at the different sea-states are shown in Table 3. The threshold U_{GP} and scale σ_{GP} parameters increased with wave peak period and wave heading angle. Since central connections are subjected to stronger forces, U_{GP} and σ_{GP} were also higher. Shape parameter values varied in a range of $-0.1 > \bar{k}_{GP} > -0.2$, however, it was close to zero at Sea State 9.

Of the two peak selection methods, the overall best fit was found when the Generalized Pareto distribution was fitted to data selected using the POT method. This approach is therefore recommended for fitting the wave-induced forces on the connections of the floating pontoon breakwater.

3.3.3. Design force for a 3-h sea state

In the sections above, the data from short-duration simulations (2000 s) were used to find the peak force distributions on the connections and fit them to the PDFs. Based on previous findings, two approaches were used to estimate the exceedance probability of a given wave-induced force during a 3-h sea state.

- Approach A: Applies the zero-up crossing method for peak selection, and fits the data to the Weibull PDF.
- Approach B: Applies the POT method for peak selection, and fits the data to the Generalized Pareto PDF.

The probability of exceedance of a given force on C_3 during a 3-h-long sea state (F_{3h}) after applying both approaches is shown at all the sea states in Fig. 15. In general, the exceedance distributions found with Approach B are skewed more to the right than those found with Approach A. It therefore follows that Approach A may underestimate the wave-induced forces on the connections.

The design loads at two different levels of exceedance probability

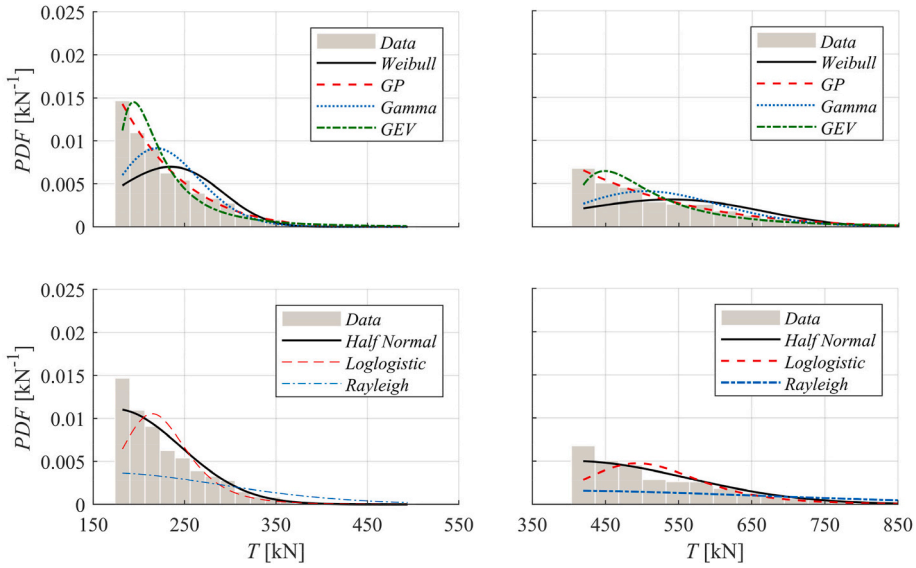

Fig. 13. Histograms of force peaks selected with the Peaks Over Threshold (POT) method and fit to Probability Density Functions (PDFs) for Connections C_1 (left) and C_3 (right) at sea-state 6 ($T_p = 6.0$ s and $\theta = 67.5°$).

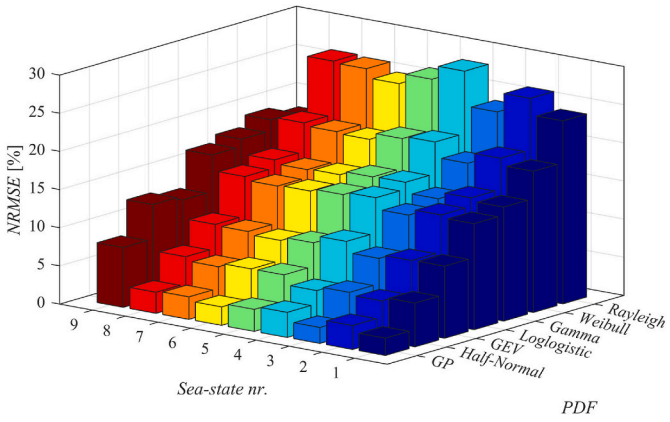

Fig. 14. Average NMRSE between the force peak data found with the Peaks Over Threshold (POT) method and different PDF models at the sea states considered.

($T_{0.63}$ and $T_{0.10}$, as defined in Section 2.3.3) are summarized in Table 4 for both approaches. Since the intermediate connections of the array were expected to withstand higher forces, those results have been selected for discussion. As described above, wave-induced forces increased with the wave peak period and heading angle.

As shown in Fig. 15, Approach B resulted in a higher design force than Approach A ($T_{0.63}$ increased from 74% to 200% and $T_{0.10}$ increased from 17 to 105%, depending on the sea state). The one exception to this pattern is conflictive Sea State 9 above. In this case, Approach A yielded a slightly higher value for $T_{0.63}$ and a much higher value for $T_{0.10}$. The poor fits to this sea state with both approaches may be the reason for this result.

With Approach B, the maximum design forces were expected for Sea State 9 ($T_p = 9$ s and $\theta = 67.5°$), with $T_{0.63} = 879.3$ kN and $T_{0.10} = 917.2$ kN, and the minimums were expected for Sea State 1 ($T_p = 3$ s and $\theta = 22.5°$), with $T_{0.63} = 79.0$ kN and $T_{0.10} = 89.8$ kN. As observed, there was a significant difference in the wave-induced forces at these two sea states. A similar trend was found for the results with Approach A, confirming the influence of the wave parameters on the design connection forces.

Applying Approach A resulted in much wider differences in $T_{0.63}$ and $T_{0.10}$ (64–71%, Table 4) than with Approach B (less than 12%). It may therefore be inferred that the approach selected for finding the probability of exceedance, i.e. the peak selection criterion and the PDF applied for fitting the peaks, has a stronger influence on the design value of the wave-induced forces on the connections than the selection of one probability of exceedance or another.

4. Conclusions

The literature lacks well-stablished recommendations and standards for the design of floating pontoon breakwaters, and in particular, the connections between modules. This article therefore proposed and developed a methodology for defining the wave-induced forces on the connections. For this purpose, an array of five floating pontoons

Table 3
Generalized Pareto distribution parameters (average ± standard deviation) found for terminal (C_1, C_2, C_7 and C_8) and intermediate (C_3, C_4, C_5 and C_6) connections.

Sea state No.	Terminal			Intermediate		
	$\overline{U}_{GP}$	$\overline{k}_{GP} \times 10^{-3}$	$\overline{\sigma}_{GP}$	$\overline{U}_{GP}$	$\overline{k}_{GP} \times 10^{-3}$	$\overline{\sigma}_{GP}$
1	32.3 ± 5.8	−159.0 ± 21.9	12.3 ± 2.0	57.2 ± 2.7	−171.9 ± 8.4	23.4 ± 1.0
2	57.3 ± 6.4	−173.2 ± 31.7	21,3 ± 2.3	86.2 ± 4.0	−178.6 ± 18.7	32.7 ± 1.2
3	116.4 ± 8.4	−142.7 ± 18.8	42,8 ± 3.9	162.9 ± 7.7	−148.7 ± 25.0	60.4 ± 1.6
4	54.2 ± 5.4	−182.3 ± 30.2	18,4 ± 2.1	88.1 ± 3.1	−200.2 ± 24.6	28.7 ± 1.7
5	102.3 ± 6.9	−148.7 ± 31.1	33,8 ± 1.8	172.0 ± 2.5	−173.7 ± 23.8	57.2 ± 1.4
6	179.0 ± 5.1	−138.9 ± 20.7	58,6 ± 2.7	406.8 ± 3.0	−158.6 ± 17.0	134.2 ± 5.1
7	49.8 ± 6.1	−140.6 ± 16.8	15,2 ± 2.4	96.9 ± 5.1	−159.9 ± 45.6	30.1 ± 1.7
8	103.3 ± 4.1	−149.7 ± 15.7	30,6 ± 1.3	210.9 ± 2.8	−153.1 ± 17.7	66.2 ± 2.7
9	387.1 ± 20.1	27.5 ± 18.9	461,7 ± 38.8	727.4 ± 8.5	−340.2 ± 31.0	864.1 ± 43.7

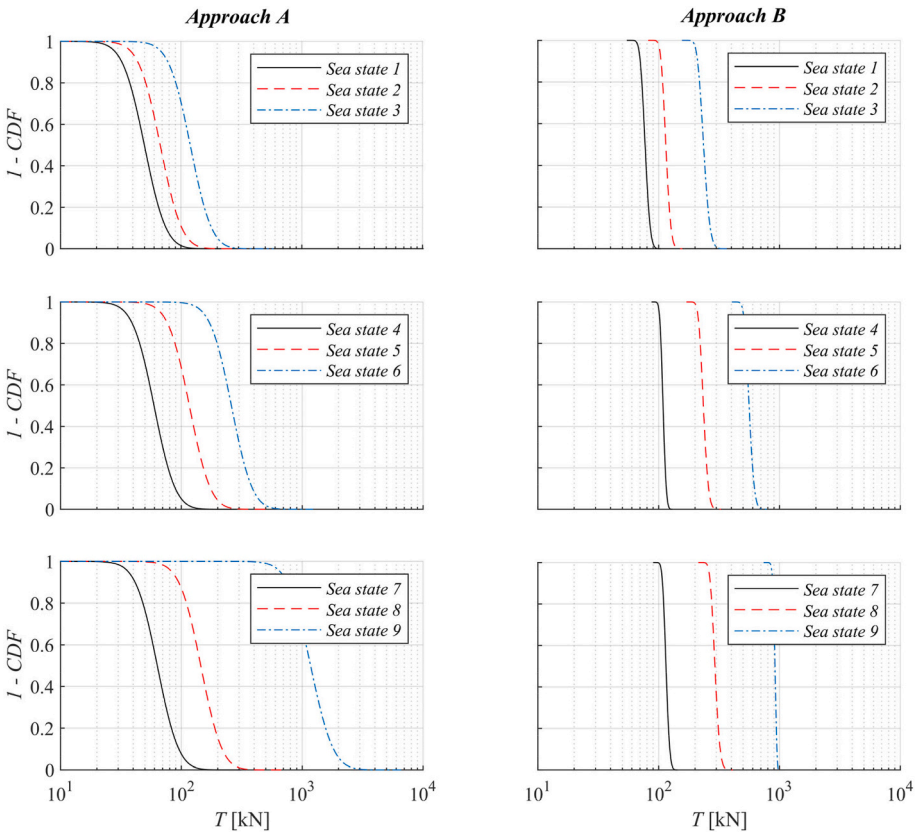

Fig. 15. Probability of exceedance of a given force (T) in a 3-h sea state (F_{3h}) found with Approach A (zero-up crossing method and Weibul distribution, left) and with Approach B (POT method and generalized Pareto Distribution, right) on Connection C_3.

Table 4
Average design wave-induced force on Connections C_3, C_4, C_5 and C_6 for two exceedance probabilities.

Sea state			Approach B (Zero-up crossing and Weibull distribution)		Approach A (POT and Generalized Pareto distribution)	
No.	T_p [s]	θ [°]	$\overline{T}_{0.63}$ [kN]	$\overline{T}_{0.10}$ [kN]	$\overline{T}_{0.63}$ [kN]	$\overline{T}_{0.10}$ [kN]
1	3	22.5	45.5	76.7	79.0	89.8
2	3	45.0	62.3	104.8	115.5	129.7
3	3	67.5	107.2	179.7	229.1	264.0
4	6	22.5	53.4	89.3	110.4	120.8
5	6	45.0	104.70	174.8	225.0	251.1
6	6	67.5	233.41	388.4	543.8	613.8
7	9	22.5	56.8	95.3	128.4	145.1
8	9	45.0	130.1	217.4	281.0	317.3
9	9	67.5	1048.0	1817.6	879.3	917.2

interconnected by hinged joints and anchored to the seabed with elastic mooring lines was analysed. The hydrodynamics and wave-structure interactions were solved by a time-domain numerical model for nine sea states with different wave peak periods and oblique wave directions. The time series found from the short-duration simulations (2000 s) were used to calculate the forces associated with different exceedance levels during a typical 3-h sea state, which could be considered design wave-induced forces.

Two peak selection methods, zero-up crossing and POT, were applied and compared. The best functions for fitting the peak dataset were the Weibull and the Pareto, respectively. For the POT method, the 75th percentile of the force peaks found with the Zero-up Crossing method was considered the threshold, as in general, it provided the best fits.

The analysis confirmed that not only the wave parameters, but also the position of the connection in the floating breakwater is critical to wave-induced forces, as suggested in previous publications. At the sea states considered, the wave-induced forces on the connections increased with peak wave period and obliquity, and intermediate connections withstood much higher forces than terminal connections.

Two approaches were applied and compared for extreme value analysis of the wave-induced forces on the connections.

- Approach A, which applied the zero-up crossing method for the selection of peaks and data fit to the Weibull PDF.
- Approach B, which applied the POT method for peak selection and fit the data to the Generalized Pareto PDF.

Approach A resulted in poorer fit to the force datasets and lower wave-induced force design values. Therefore, as Approach A may underestimate extreme force values, Approach B is recommended for defining the design wave-induced forces on the connections of floating pontoon breakwaters.

Moreover, the differences in design force values found with the two methods were greater than the differences found when using one probability of exceedance or another (63rd and 90th percentiles). Therefore, the application of appropriate peak selection methods in combination with a PDF was found to be paramount.

Summarizing, this article provides guidelines for designing floating breakwaters, including a complete methodology for estimating the extreme wave-induced forces on the connections, the keystone in the design of these structures. Future research should focus on fatigue damage to these elements, which may compromise the lifetime of the entire structure.

CRediT authorship contribution statement

A.J. Cebada-Relea: Conceptualization, Methodology, Software, Formal analysis, Investigation, Resources, Writing – original draft, Writing – review & editing, Visualization. **M. López:** Conceptualization, Methodology, Software, Formal analysis, Investigation, Resources, Writing – original draft, Writing – review & editing, Visualization, Supervision, Project administration, Funding acquisition. **R. Claus:** Conceptualization, Formal analysis, Writing – original draft, Writing – review & editing. **M. Aenlle:** Conceptualization, Methodology, Investigation, Supervision, Funding acquisition.

Declaration of competing interest

The authors declare that they have no known competing financial interests or personal relationships that could have appeared to influence the work reported in this paper.

Data availability

Data will be made available on request.

Acknowledgments

A. Cebada received financial aid from the University of Oviedo (Asturias, Spain) under the 2021 Research Aid and Promotion Plan ("*Ayudas para realización de Tesis Doctorales. Modalidad A: Contratos de Investigación en régimen de concurrencia competitiva.*" [Grant for PhD Students, Unit A: Research Contracts with Competitive Funding], Ref. PAPI-21-PF-31).

References

Agarwal, P., Walker, W., Bhalla, K., 2015. Estimation of Most Probable Maximum from Short-Duration or Undersampled Time-Series Data, pp. 1–8. https://doi.org/10.1115/omae2015-41701.

ANSYS, 2016. ANSYS Aqwa. ANSYS Ltd., Canonsburg, PA, USA.

Cebada Relea, A.J., López Gallego, M., Claus Gómez, R., Soto Pérez, F., 2022. Numerical Investigation of Floating Breakwaters Using Time Domain Boundary Element Method. In: Proc. of the 39th IAHR World Congress (Granada, 2022), p. 4383. https://doi.org/10.3850/IAHR-39WC252171192022379.

Cebada-Relea, A.J., López, M., Aenlle, M., 2022a. Time-domain numerical modelling of the connector forces in a modular pontoon floating breakwater under regular and irregular oblique waves. Ocean Eng. 243, 110263 https://doi.org/10.1016/j.oceaneng.2021.110263.

Cebada-Relea, A., López, M., Soto, F., Claus, R., 2022b. Diques flotantes portuarios: análisis las conexiones y sinergias con la energía undimotriz. Revista española de la Fractura 3, 199–204.

Chen, X., Miao, Y., Tang, X., Liu, J., 2017. Numerical and experimental analysis of a moored pontoon under regular wave in water of finite depth. Ships Offshore Struct. 12, 412–423. https://doi.org/10.1080/17445302.2016.1172831.

Cheng, Z., Kuang, J., 2016. Extreme response predictions for deepwater mooring system. In: Offshore Technol Conf Asia 2016, OTC-26423-MS. https://doi.org/10.4043/26423-ms.

Chu, Y.I., Wang, C.M., Zhang, H., 2022. A frequency domain approach for analyzing motion responses of integrated offshore fish cage and wind turbine under wind and wave actions. Aquacult. Eng. 97, 102241 https://doi.org/10.1016/j.aquaeng.2022.102241.

Cummins, W.E., 1962. The Impulse Response Function and Ship Motions, vol. 57. DTIC Document. https://doi.org/10.1179/2056711115Y.00000000001.

Dai, J., Wang, C.M., Utsunomiya, T., Duan, W., 2018. Review of recent research and developments on floating breakwaters. Ocean Eng. 158, 132–151. https://doi.org/10.1016/j.oceaneng.2018.03.083.

Diamantoulaki, I., Angelides, D.C., 2010. Analysis of performance of hinged floating breakwaters. Eng. Struct. 32, 2407–2423. https://doi.org/10.1016/j.engstruct.2010.04.015.

Diamantoulaki, I., Angelides, D.C., 2011. Modeling of cable-moored floating breakwaters connected with hinges. Eng. Struct. 33, 1536–1552. https://doi.org/10.1016/j.engstruct.2011.01.024.

DNV GL, 2017. DNVGL-RP-C205: environmental conditions and environmental loads.

DNV GL, 2018. DNVGL-CG-0130: Wave Loads.

Elchahal, G., Lafon, P., Younes, R., 2009. Design optimization of floating breakwaters with an interdisciplinary fluid-solid structural problem. Can. J. Civ. Eng. 36, 1732–1743. https://doi.org/10.1139/L09-095.

Ferreras, J., Peña, E., López, A., López, F., 2014. Structural performance of a floating breakwater for different mooring line typologies. J. Waterw. Port, Coast. Ocean Eng. 140, 1–11. https://doi.org/10.1061/(ASCE)WW.1943-5460.0000240.

Lee, J., Cho, W., 2003. Hydrodynamic analysis of wave interactions with a moored floating breakwater using the element-free Galerkin method. Can. J. Civ. Eng. 30, 720–733. https://doi.org/10.1139/l03-020.

Loukogeorgaki, E., Angelides, D.C., 2005. Stiffness of mooring lines and performance of floating breakwater in three dimensions. Appl. Ocean Res. 27, 187–208. https://doi.org/10.1016/j.apor.2005.12.002.

S.F. Marina (n.d).

Martinelli, L., Ruol, P., Zanuttigh, B., 2008. Wave basin experiments on floating breakwaters with different layouts. Appl. Ocean Res. 30, 199–207. https://doi.org/10.1016/j.apor.2008.09.002.

McCartney, B.L., 1985. Floating breakwater design. J. Waterw. Port, Coast. Ocean Eng. 111, 304–318. https://doi.org/10.1061/(asce)0733-950x(1985)111:2(304).

Peña, E., Ferreras, J., Sanchez-Tembleque, F., 2011. Experimental study on wave transmission coefficient, mooring lines and module connector forces with different designs of floating breakwaters. Ocean Eng. 38, 1150–1160. https://doi.org/10.1016/j.oceaneng.2011.05.005.

Rajesh Reguram, B., Surendran, S., Lee, S.K., 2016. Application of fin system to reduce pitch motion. Int. J. Nav. Archit. Ocean Eng. 8, 409–421. https://doi.org/10.1016/j.ijnaoe.2016.05.004.

Ramos, V., López, M., Taveira-Pinto, F., Rosa-Santos, P., 2018. Performance assessment of the CECO wave energy converter: water depth influence. Renew. Energy 117, 341–356. https://doi.org/10.1016/j.renene.2017.10.064.

Richey, E.P., 1982. Floating Breakwater Field Experience. Coastal Engineering Research Center, Vicksburg, MS (US).

Samaei, S., Azarsina, F., Ghahferokhi, M., 2016. Numerical simulation of floating pontoon breakwater with ANSYS AQWA software and validation of the results with laboratory data. Bull. La Société R Des. Sci. Liège 85, 1487–1499.

Sinsabvarodom, C., Leira, B.J., Chai, W., Næss, A., 2021. Short-term extreme mooring loads prediction and fatigue damage evaluation for station-keeping trials in ice. Ocean Eng. 242, 109930 https://doi.org/10.1016/j.oceaneng.2021.109930.

Stanisic, D., Efthymiou, M., Kimiaei, M., Zhao, W., 2017. Evaluation of conventional methods of establishing extreme mooring design loads. Proc. Int. Conf. Offshore Mech. Arct. Eng.OMAE 3A-2017, 2–10. https://doi.org/10.1115/OMAE201761243.

Stanisic, D., Efthymiou, M., Kimiaei, M., Zhao, W., 2018. Design loads and long term distribution of mooring line response of a large weathervaning vessel in a tropical cyclone environment. Mar. Struct. 61, 361–380. https://doi.org/10.1016/j.marstruc.2018.06.004.

Williams, A.N., Lee, H.S., Huang, Z., 2000. Floating pontoon breakwaters. Ocean Eng. 27, 221–240. https://doi.org/10.1016/S0029-8018(98)00056-0.

Xu, S., Guedes Soares, C., 2021. Bayesian analysis of short term extreme mooring tension for a point absorber with mixture of gamma and generalised pareto distributions. Appl. Ocean Res. 110, 102556 https://doi.org/10.1016/j.apor.2021.102556.

Xu, S., yan, Ji C., Guedes Soares, C., 2019. Estimation of short-term extreme responses of a semi-submersible moored by two hybrid mooring systems. Ocean Eng. 190, 106388 https://doi.org/10.1016/j.oceaneng.2019.106388.

Xu, S., Wang, S., Guedes Soares, C., 2020. Experimental investigation on hybrid mooring systems for wave energy converters. Renew. Energy 158, 130–153. https://doi.org/10.1016/j.renene.2020.05.070.

Zhao, Y., Liao, Z., Dong, S., 2021. Estimation of characteristic extreme response for mooring system in a complex ocean environment. Ocean Eng. 225, 108809 https://doi.org/10.1016/j.oceaneng.2021.108809.